Characterization of ultrasound contrast microbubbles using *in vitro* experiments and viscous and viscoelastic interface models for encapsulation

Kausik Sarkar[a)]
Department of Mechanical Engineering, University of Delaware, Newark, Delaware 19716

William T. Shi
Department of Radiology, Thomas Jefferson University, Philadelphia, Pennsylvania 19107 and Philips Research, Briarcliff Manor, New York 10510

Dhiman Chatterjee
Department of Mechanical Engineering, University of Delaware, Newark, Delaware 19716 and Department of Mechanical Engineering, IIT Madras, Chennai 600036, India

Flemming Forsberg
Department of Radiology, Thomas Jefferson University, Philadelphia, Pennsylvania 19107

(Received 20 August 2004; revised 30 March 2005; accepted 6 April 2005)

Zero-thickness interface models are developed to describe the encapsulation of microbubble contrast agents. Two different rheological models of the interface, Newtonian (viscous) and viscoelastic, with rheological parameters such as surface tension, surface dilatational viscosity, and surface dilatational elasticity are presented to characterize the encapsulation. The models are applied to characterize a widely used microbubble based ultrasound contrast agent. Attenuation of ultrasound passing through a solution of contrast agent is measured. The model parameters for the contrast agent are determined by matching the linearized model dynamics with measured attenuation data. The models are investigated for its ability to match with other experiments. Specifically, model predictions are compared with scattered fundamental and subharmonic responses. Experiments and model prediction results are discussed along with those obtained using an existing model [Church, J. Acoust. Soc. Am. **97**, 1510 (1995) and Hoff *et al.*, J. Acoust. Soc. Am. **107**, 2272 (2000)] of contrast agents. © *2005 Acoustical Society of America.* [DOI: 10.1121/1.1923367]

PACS number(s): 43.80.Qf, 43.80.Ev, 43.25.Yw, 43.35.Wa [CCC] Pages: 539–550

I. INTRODUCTION

Microbubble based contrast enhancing agents can achieve significant improvement of ultrasound images of blood flow (Goldberg *et al.*, 2001; Frinking *et al.*, 2000). These bubbles are encapsulated by a layer of surface active materials such as lipids or proteins to stabilize them against premature dissolution in the blood stream (Goldberg *et al.*, 2001; Frinking *et al.*, 2000). The performance of these contrast agents *in vivo* depends on their interaction with the incident acoustic pressure. The encapsulation plays a significant role in this interaction. Accurate characterization of contrast agent behavior therefore critically relies on a good model of the encapsulation. *In vitro* attenuation and scattering experiments have been performed on various contrast agents (e.g., Albunex®, Molecular Biosystems Inc., San Diego, CA; Optison® GE Healthcare, Princeton, NJ; Sonazoid® GE Healthcare, Oslo, Norway; Definity® of Bristol-Myers Squibb Medical Imaging, N. Billerica, MA) to understand and characterize their properties (see, for example, Hoff *et al.*, 2000; de Jong *et al.*, 1992; de Jong and Hoff, 1993; Frinking and de Jong, 1998; Shi *et al.*, 1999; Morgan *et al.*, 2000). Recently, nonlinear contrast behaviors, both second- and sub-harmonic responses, have been studied by many researchers (Shi *et al.*, 1999; Simpson *et al.*, 1999; Chang *et al.*, 1996; de Jong *et al.*, 1994; Shankar *et al.*, 1998; Shi and Forsberg, 2000). Contrast agents exhibit stronger nonlinear response than the surrounding tissue. The enhanced nonlinear response is harnessed to improve contrast-to-tissue signal in various nonlinear imaging modalities such as harmonic, subharmonic, pulse inversion, or power Doppler imaging.

A number of models for contrast agents have been developed modifying the free bubble dynamics equation [see, e.g., Leighton (1994), p. 303] for the presence of encapsulation. de Jong and co-workers (de Jong *et al.*, 1992; de Jong and Hoff, 1993; Frinking and de Jong, 1998) initiated systematic contrast agent modeling with one of the first clinically approved agents, Albunex. They assumed the encapsulating shell to be made of a viscoelastic solid, and used lumped parameters in the free bubble equation to model its effects. Church (1995) provided a detailed theoretical model of contrast agents by treating the encapsulating shell as a nanometer thick layer of an incompressible rubbery medium with shear elasticity and viscosity. He demonstrated the sig-

[a)]Electronic mail: sarkar@me.udel.edu

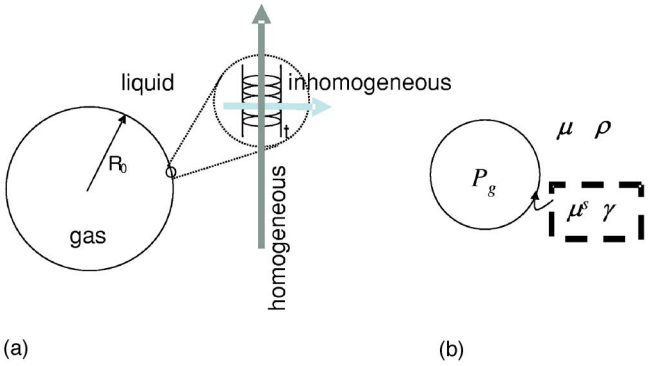

FIG. 1. (a) Schematic of a typical encapsulated bubble; R_0 is the initial bubble radius and t, the thickness of encapsulation. $t \ll R_0$. Due to the presence of molecules, the layer is inhomogeneous in the thickness direction unlike the in-plane directions. (b) The interface model with surface rheology. The gas is modeled as a bulk medium with a uniform gas pressure P_g. The outside liquid is also modeled as a bulk medium with density ρ and viscosity μ. The interface is taken to be a sharp interface of zero thickness, and endowed with intrinsic rheological properties surface viscosity (μ^s) and surface tension (γ).

nificance of the shell parameters by varying them over a wide range, and obtained fundamental and second-harmonic response by a perturbation method, but did not try to experimentally relate the model parameters to any specific contrast agent. Introducing slight compressibility and viscoelasticity of the surrounding liquid in the same model, Khismatullin and Nadim (2002) performed a theoretical analysis to conclude that these effects are less important than that of the encapsulation. Morgan *et al.* (2000) used a modified Herring equation with a similar model for the encapsulation to compare with optical observations obtained by high-speed digital camera.

Biochemical analysis with freeze-etching and SEM observations provides the detail structure of microbubble encapsulation (Christiansen *et al.*, 1994; Myrset *et al.*, 1996; May *et al.*, 2002; El-Sherif and Wheatley, 2003). It consists of a few nanometer thick layer of one or few molecules [Fig. 1(a)], and is therefore neither homogeneous in the thickness direction, nor is it isotropic. The finite thickness model of the microbubble encapsulation proposed by various authors (Church, 1995; Morgan *et al.*, 2000; Khismatullin and Nadim, 2002) containing incompressible materials with homogeneous and isotropic bulk material property therefore might not be appropriate (Evans and Skalak, 1980; Edwards *et al.*, 1991). On the other hand, a molecular model is prohibitively expensive and is not really necessary for describing the acoustic behavior. Chatterjee and Sarkar (2003) have adopted a new interface model [Fig. 1(b)] for the encapsulation that retains continuum character only in the in-plane direction. The model interface is of zero thickness, and assumed to have rheological properties such as *interfacial* tension and surface viscosity (in contrast to *bulk* viscosity and elasticity for the material of existing finite-thickness encapsulation models). The zero thickness assumption is justified in view of the thinness ($\sim$nm) of the encapsulation compared to the bubble radius ($\sim \mu$m). It avoids making any assumptions about the structure along the thickness direction of encapsulation, but the interface rheology captures its essential effects. Such an approach has been used for fluid interfaces with adsorbed surfactants and proteins (Graham and Phillips, 1980), a case very similar to the present one. The validity of any model has to be established by successful comparison with independent experimental observations. To date a comparative investigation into predictive capabilities of different models has not been performed.

Applying a Newtonian viscous rheology for the interface, Chatterjee and Sarkar (2003) have obtained interfacial properties (surface tension $\gamma = 0.9$ N/m, surface dilatational viscosity $\kappa^s = 0.08$ msP) of Optison (GE Healthcare, Princeton, NJ) from attenuation experiments. The model correctly predicted experimentally observed subharmonic emission from Optison measured by Shi *et al.* (1999). However, while one would expect the surface tension value to decrease due to adsorption of surface active materials, $\gamma = 0.9$ N/m determined by matching with experiment is much higher than that (~ 0.07 N/m) of a pure gas–water interface. They ascribed the large surface tension to the inadequacy of the Newtonian model for the encapsulation rheology. In the absence of an explicit surface elasticity term, all elastic effects were lumped in the surface tension term. The observation warrants introduction of a non-Newtonian viscoelastic interfacial rheology for the encapsulation.

In this paper, we develop such a viscoelastic interface model for the encapsulation of a thin-shelled contrast microbubble. We perform an *in vitro* acoustic investigation of contrast agent Sonazoid (GE Healthcare, Oslo, Norway), and apply both Newtonian (viscous) and viscoelastic models to it. Sonazoid (also known as NC100100) consists of fluorocarbon gas microbubbles with a flexible surfactant membrane. The bubble size distribution is relatively narrow with a median diameter of 3.2 μm (Sontum *et al.*, 1999). Sonazoid is a widely studied contrast agent. Recently, possibility of inertial cavitation following Sonazoid bubble destruction was investigated by Shi *et al.* (2000). Moran *et al.* (2002) investigated this agent at an intravascular imaging frequency of 30 MHz. Here, we perform attenuation at different dilutions of Sonazoid. Independently, we measure scattering at various frequencies and amplitudes. We develop interface models for the microbubble encapsulation using two rheologies, and obtain corresponding Rayleigh–Plesset type of equations for bubble radius. We determine the surface parameters using the experimental attenuation data. For comparison, we also compute similar results for the Church's shell model using a formulation appropriate for a thin shell as presented by Hoff *et al.* (2000) [Eq. 6 in their paper; this model hereafter is referred to as Church–Hoff's model]. Using the model parameters, we solve the Rayleigh–Plesset equation to determine the scattered response of the models. Measured fundamental and sub-harmonic scatterings are compared with the numerical model predictions. A detailed comparative study of the various model behaviors and their ability to predict experimental measurement is presented.

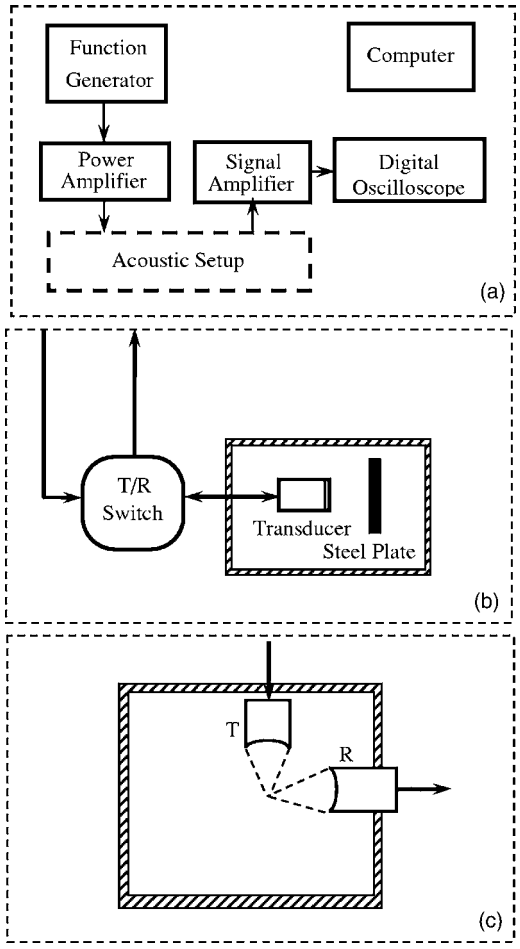

FIG. 2. Experimental setup for measuring attenuation and scattering.

II. EXPERIMENTAL SETUP AND METHOD

A. Experimental setup for measuring attenuation

A pulse-echo system was employed for measuring attenuation of ultrasound in a solution of contrast agent. The block diagrams of its electronic and acoustic arrangements are shown in Figs. 2(a) and 2(b), respectively. A programmable function generator (model 8116A; Hewlett Packard, Santa Clara, CA) produced short pulses at a pulse repetition frequency (PRF) of 10 Hz for transmission. The transmit signals were first amplified in a broadband 50 dB rf power amplifier (model 325LA; ENI, Rochester, NY) [Fig. 2(a)] and then supplied to a single-element broadband flat transducer (Etalon, Lebanon, IN) through an electronic Transmit/Receive switch (model RDX-6; Ritec, Warwick, RI) with a double-mixer range gate [see Fig. 2(b)]. The transducer had a diameter of 12.2 mm, a center frequency of 3.6 MHz, and a bandwidth (6 dB down from maximum) of 98%. A flat stainless steel plate was placed in front of the transducer as an acoustic reflector [Fig. 2(b)]. Reflected ultrasound pulses were received by the same transducer, and the received signals were amplified with a low noise rf amplifier (model 5052 PR; Panametrics, Waltham, MA). The amplified signals were acquired at a sampling frequency of 50 MHz using a digital oscilloscope equipped with mathematical functions (model 9350AM; LeCroy, Chestnut Ridge, NY). For each measurement, 64 sequences of 20 μs scattered signals were taken at the PRF of 10 Hz. An average spectrum of these 64 data sequences was then obtained using a FFT function in the oscilloscope. The average power spectrum was transferred via an IEEE-488 interface to a PowerPC for further analysis. The communication with the function generator and the data transfer from the digital oscilloscope were controlled by LABVIEW® (National Instruments, Austin, TX). The acoustic attenuation of diluted Sonazoid, as a function of frequency, was determined by subtracting the average spectrum prior to injection of the agent from the spectrum obtained after injection. Each attenuation measurement took less than 10 s. Similar attenuation measurement was performed by other investigators (see, e.g., Hoff *et al.*, 2000).

B. Experimental setup for measuring scattering

As shown in Fig. 2(c), an acoustic arrangement with two transducers (transmitter and receiver) was employed. All transducers were single element spherically focused transducers with a diameter of 12.2 mm and a focal length of 2.5 cm. One transducer (R1-4025; Etalon) with a bandwidth of 86% and a center frequency of 3.6 MHz was used as the transmitter [T in Fig. 2(c)] for insonation at frequencies of 2.0, 3.0, 4.4, and 6.0 MHz. The second transducer (C1-4035; Etalon) with a bandwidth of 120% and a center frequency of 6.2 MHz was used as the receiver [R in Fig. 2(c)]. The transmit transducer was positioned confocally at right angle to the receiving transducer. Since contrast microbubbles are much smaller than the acoustic wavelength and undergo volume pulsation in an ultrasound field, scattered signals received at 90° should be very similar to the backscattered echoes (Shi *et al.*, 2000). The advantage of this measurement system is its high spatial resolution. This is because scattered signals only come from the microbubbles in the small overlapping confocal region of the transmitting and receiving transducers.

For each measurement, ultrasound sine-wave tonebursts with 64 cycles were transmitted at a PRF of 10 Hz. A sequence of 64 scattered signals, each of 50 μs duration, was acquired using the LeCroy digital oscilloscope with a sampling frequency of 50 MHz. Acquired data were transferred via an IEEE-488 interface to a PC (Dell, Austin, TX) and processed using a FFT spectrum analyzer with Hamming window in LABVIEW. All spectra of scattered signals were averaged over 64 data sequences. The transient effects are limited only to the initial cycles, and the computed subharmonic response is independent of the pulse length (Shi *et al.*, 1999).

All measurements were carried out at room temperature (around 25 °C). Isoton® II (Coulter, Miami, FL) was utilized as the buffer for the contrast agent solution. It was kept in circulation by a magnetic stirrer. The acoustic output of the transmit transducer was calibrated in water using a 0.5 mm broadband acoustic needle hydrophone (Precision Acoustics, Dorchester, UK).

III. MATHEMATICAL FORMULATION

A. Interfacial rheology models for encapsulation and encapsulated bubble dynamics

The encapsulation of a contrast agent is made of a few layers (often a monolayer) of molecules (Fig. 1). As mentioned in Sec. I, such a layer is not homogeneous in the thickness direction and therefore neither is it isotropic. However, the encapsulation can be considered a macroscopic homogeneous continuum in the other two directions (Evans and Skalak, 1980; Edwards *et al.*, 1991). Due to its much smaller thickness compared to the bubble radius, we assume it to be an interface of infinitesimal thickness. It is endowed with intrinsic interface properties "that represents the effects integrated over the composite molecular structure in the thickness direction" (Evans and Skalak, 1980, p. 2). Biological membranes and fluid interfaces with adsorbed surfactants and proteins (Evans and Skalak, 1980; Edwards *et al.*, 1991; Graham and Phillips, 1980) have been modeled with such an interface. The interface gives rise to interfacial stresses that are to be modeled by interface rheology. The rationale for using zero-thickness interface models is stronger in case of thin-shelled contrast microbubbles. The thickness of the encapsulation is 4 nm for Sonazoid microbubble, whereas its mean diameter is 3.2 μm (Sontum *et al.*, 1999).

A micron size bubble in an acoustic pressure field of 1 MHz (the radius to wavelength ratio is $\sim 10^{-3}$) can be assumed to retain its spherical shape as the pressure varies little over the bubble surface. Substantial shape deformation, e.g., in case of microbubble breakup, is not considered in this model. Assuming spherical symmetry, the mass and momentum conservation equations in the surrounding liquid are

$$\frac{1}{r^2}\frac{\partial}{\partial r}(r^2 v_r) = 0, \tag{1}$$

$$\rho\left(\frac{\partial v_r}{\partial t} + v_r\frac{\partial v_r}{\partial r}\right) = -\frac{\partial p}{\partial r} + \mu\left[\frac{1}{r^2}\frac{\partial}{\partial r}\left(r^2\frac{\partial v_r}{\partial r}\right) - \frac{2v_r}{r^2}\right], \tag{2}$$

where v_r is the radial component of velocity, ρ the liquid density, p the pressure, and μ is the liquid viscosity. Note that incompressibility is assumed for the surrounding liquid. Effects of liquid compressibility and viscoelasticity have been investigated by Khismtullin and Nadim (2002) by a matched asymptotic technique and found to be small. We also examined the effects of compressibility on the characterization (see Sec. IV). From mass conservation (1), the radial velocity in the liquid is readily obtained as that due to a potential source:

$$v_r = \dot{R}R^2/r^2, \tag{3}$$

where R is the radius of the bubble. Note that the velocity being irrotational, the viscous terms vanish identically. Using Eq. (3), Eq. (2) can be integrated to give at $r=R$,

$$\rho\left(R\ddot{R} + \frac{3}{2}\dot{R}^2\right) = p_{r=R} - p_\infty, \tag{4}$$

where $p_{r=R}$ is the pressure in the liquid immediately outside the bubble, and p_∞ is the liquid pressure far away:

$$p_\infty = P_0 - p_A(t), \tag{5}$$

P_0 is the liquid hydrostatic pressure and $p_A(t)$ is the excitation pressure. The dynamic boundary condition at the bubble interface relates the pressure $p_{r=R}$ to the bubble dynamics.

1. Newtonian interfacial rheological model

The dynamic condition at the interface $r=R$ can be obtained by considering the force balance in a thin lamina containing the segment of the interface. Similar to the flow in the bulk, one can model the stresses at an interface by a constitutive equation. For a Newtonian interfacial rheology, the surface extra stress and the jump in the bulk viscous stress across the interface arising from the force balance are (Edwards *et al.*, 1991, p. 109)

$$\begin{aligned} &\tau_s = \gamma I_s + (\kappa^s - \mu^s)(I_s{:}D_s)I_s + 2\mu^s D_s, \\ &[\tau\cdot\mathbf{n}]_{\text{surface}} = \nabla_s\cdot\tau_s, \end{aligned} \tag{6}$$

where γ is the surface tension, κ^s and μ^s are interfacial dilatational and shear viscosities, I_s and D_s are the surface identity and surface strain rate tensors (Edwards *et al.*, 1991). The center dot represents a scalar product between two second-order tensors. The motion inside the bubble is neglected, and a spatially uniform interior pressure $P_G(t)$ is assumed. One can use the radial part of the jump condition (6) to obtain (see Edwards *et al.*, 1991, p. 114)

$$\begin{aligned} \left(-p + 2\mu\frac{\partial v_r}{\partial r}\right)_{r=R} + P_G &\equiv -p_{r=R} - 4\mu\frac{\dot{R}}{R} + P_G \\ &= \frac{2\gamma}{R} + \frac{4\kappa^s\dot{R}}{R^2}. \end{aligned} \tag{7}$$

For a free bubble, dilatational viscosity κ^s, which arises due to the encapsulation, is zero, and γ is at its clean surface value. The surface shear viscosity does not appear due to the spherical symmetry of the dynamics. The (dilatational) viscous term can be explained by noting that the bubble undergoes area dilation at a rate $A^{-1}dA/dt = 2\dot{R}/R, (A = 4\pi R^2)$. It results in a uniform tension of magnitude $2\kappa^s\dot{R}/R$ in Eq. (7), in addition to the surface tension γ. In an undisturbed condition (zero motion), using $p_{r=R} = P_0$ [see Eqs. (4) and (5), from Eq. (7) we obtain the initial gas pressure inside the bubble:

$$P_{G0} \equiv P_G(t=0) = P_0 + \frac{2\gamma}{R_0}, \tag{8}$$

where R_0 is the initial radius. Note that P_{G0} is not in equilibrium with the outside pressure P_0. In fact for a micron radius, the inside bubble pressure could be significantly higher depending on surface tension, leading to quick dissolution due to gas diffusion (Epstein and Plesset, 1950; Kabalnov et al., 1998; Chen et al., 2002). For this model the stability of the microbubble has to depend on the low solubility of the gas in the surrounding liquid, and more importantly on the low permeability of the encapsulation, making it an effective barrier to gas diffusion.

With the Newtonian rheology, the encapsulation is purely viscous characterized by γ and κ^s. As we saw in the case of Optison (Chatterjee and Sarkar, 2003), and also will see in the following, such a model for the encapsulation results in an unusually high value for surface tension. Adsorption of small amount of surface active materials leads normally to a reduction in surface tension from its value at a clean interface. At low surface concentrations, the adsorbed molecules behave like a perfect gas; their random motion leads to an osmotic pressure acting against the surface tension. The surface tension reduction can be modeled by Gibb's adsorption isotherm that is identical to the perfect gas law (Edwards *et al.*, 1991, p.25). However, in an encapsulation the molecules are at a high concentration and closely packed, with a strong attractive interaction between them, making the "ideal gas" law invalid. Due to the attractive interaction, any change in area will lead to an elastic force, a phenomenon commonly known as Gibb's elasticity [see Evans and Skalak (1980), pp. 80 and 86 and Edwards *et al.* (1991), pp. 118 and 172]. A Newtonian constitutive equation assumes that the deviatoric part of stress is entirely of viscous origin and has only an isotropic surface pressure term, namely the surface tension (Kralchevsky and Nagayama, 2001, p. 158). While fitting the experimental observation, all elastic effects get lumped into it, generating the high value. The resulting mechanical surface tension is significantly different from its thermodynamic value, and can alternately be interpreted as an effective parameter to represent all "elastic" effects (usual thermodynamic tension in the surface as well as dilatational elasticity arising from fractional increase in area over unstressed configuration) of the shell.

2. Viscoelastic interfacial rheological model

The above observation indicates the need for a viscoelastic rheology with explicit surface elasticities. Edwards *et al.* (1991, p.118) has shown that dilatational surface elasticity or Gibb's elasticity can also be treated as effects arising from surface tension gradients. Accordingly, the dilatational elasticity E^s is introduced as

$$E^s = \left(\frac{\partial \gamma}{\partial \alpha}\right)_{\beta=0}, \quad \gamma = \gamma_0 + E^s \beta, \tag{9}$$

where $\beta = \delta A/A = [(R/R_E)^2 - 1]$ is the fractional change in area from *equilibrium* that represents an unstrained equilibrium condition (denoted by unstrained radius R_E). γ_0 is the reference surface tension at zero area change. Note that in our Newtonian (purely viscous) approach the dynamics does not have such a reference unstrained state. A note of caution is warranted for the terminology. Edwards et al. (1991, p.118) states that because dilatational elasticity can be treated as a surface tension gradient effect, "such elastic behavior does not necessarily violate Newtonian model of interfacial rheological behavior." However, for clarity, we call the model with dilatational elasticity non-Newtonian or viscoelastic, and the one without explicit elasticity Newtonian. Evans and Skalak (1980, p.80) offered a similar model for membrane surface elasticity (they called E^s the area compressibility modulus). With the modification to surface tension γ, the dynamic boundary condition (7) at $r=R$ becomes

$$p_{r=R} = P_G - 4\mu\frac{\dot{R}}{R} - \frac{4\kappa^s \dot{R}}{R^2} - \frac{2\gamma_0}{R} - \frac{2E^s}{R}\left[\left(\frac{R}{R_E}\right)^2 - 1\right]. \tag{10}$$

At the initial zero motion state, the inside pressure satisfies

$$P_{G0} = P_0 + \frac{2\gamma_0}{R_0} + \frac{2E^s}{R_0}\left[\left(\frac{R_0}{R_E}\right)^2 - 1\right]. \tag{11}$$

In contrast to the Newtonian rheology [see Eq. (8)], we assume an *equilibrium of pressure* inside and outside the bubble $P_{G0}=P_0$, that ensures stability of microbubbles, even if the encapsulation is permeable to the gas. Imposing pressure equilibrium, we obtain the equilibrium radius

$$R_E = R_0\left(1 - \frac{\gamma_0}{E^s}\right)^{-1/2}.$$

Note that the initial radius is strained (smaller than R_E). The resulting compressive stress balances the stress due to surface tension giving rise to the pressure equilibrium.

3. Encapsulated bubble dynamics

The gas pressure inside the bubble is assumed to vary with bubble volume polytropically with k as the polytropic exponent as follows (Leighton, 1994, p.11):

$$P_G R^{3k} = P_{G0} R_0^{3k}. \tag{12}$$

P_{G0} is the gas pressure and R_0 is the initial radius. We have chosen $k=1$, corresponding to an isothermal gas behavior inside the bubble; the bubble size is too small compared to the thermal diffusion length in the time scale ($\sim 10^{-6}$ s) of oscillation (Hilgenfeldt et al., 1998). Models of heat transfer inside bubbles due to Devin (1959) and Eller (1970) indicate k to be close to unity [$\sim$1.006; see Hoff et al. (2000), their Eq. (21a)]. For the liquid–gas system, using Eqs. (5) and (10) in Eq. (4) we obtain the modified Rayleigh–Plesset equation

$$\rho\left(R\ddot{R} + \frac{3}{2}\dot{R}^2\right) = P_{G0}\left(\frac{R_0}{R}\right)^{3k} - 4\mu\frac{\dot{R}}{R} - \frac{4\kappa^s\dot{R}}{R^2} - \frac{2\gamma_0}{R} - \frac{2E^s}{R}\left[\left(\frac{R}{R_E}\right)^2 - 1\right] - P_0 + p_A(t) \tag{13}$$

for the viscoelastic interfacial rheology. Replacing Eq. (10) by Eq. (7), we obtain a similar equation for the Newtonian rheology:

$$\rho\left(R\ddot{R} + \frac{3}{2}\dot{R}^2\right) = P_{G0}\left(\frac{R_0}{R}\right)^{3k} - 4\mu\frac{\dot{R}}{R} - \frac{4\kappa^s\dot{R}}{R^2} - \frac{2\gamma}{R} - P_0 + p_A(t), \tag{14}$$

where the dilatational elasticity term is absent ($E^s=0$), and the surface tension term involves γ instead of γ_0. Equation (13) or (14) together with the initial conditions $R(t=0)=R_0$,

and $\dot{R}(t=0)=0$ describes the bubble dynamics. We conclude that (γ,κ^s) characterize a Newtonian rheology and (γ_0,E^s,κ^s) a viscoelastic rheology for the encapsulation. The second order differential equation (13) or (14) is solved using a stiff solver routine of MATLAB® (Mathwork Inc, Natick, MA).

The acoustic pressure $P_s(t)$ scattered by a bubble is (Brennen 1995, p. 83) with the assumption of incompressibility for the surrounding liquid:

$$P_s(r,t)=\rho\frac{R}{r}(2\dot{R}^2+R\ddot{R}). \tag{15}$$

The corresponding scattering cross section is given by

$$\sigma_s(t)=\frac{\langle r^2P_s(t)^2\rangle}{P_A^2}, \tag{16}$$

where the angular brackets indicate an average over a time period. Different frequency components, e.g., harmonic or subharmonic, of the scattered signal are determined by transforming the expression into frequency domain.

B. Determination of interfacial rheological parameters

The encapsulation models have unknown parameters, such as interfacial tension γ (or γ_0), dilatational viscosity κ^s, or dilatational elasticity E^s, as evident from bubble dynamics equations (13) or (14). Interfacial tension differs from its value for a pure gas–liquid interface by the presence of surfactants. The model parameters are phenomenological in nature, and must be determined experimentally. A linearized equation of motion is applied for determination purposes, by restricting the attenuation experiments to small amplitude oscillations (i.e., low excitation). The measured attenuation and scattering are integrated effects of a bubble distribution, and are difficult choices for obtaining individual bubble characteristics. Such inverse processes of parameter estimation are notorious for their ill-posed nature. We found that the linearization provides an easy and robust algorithm for the parameter determination. We also assume that the material parameters in a proper physical model are independent of the type of experiments, i.e., attenuation or scattering, and remain constant over a range of excitation frequency and amplitudes. The medical imaging is restricted to a range of frequency (~1–10 MHz), and one is justified in assuming reasonably constant properties in this frequency range. However, interface properties could vary significantly with excitation amplitudes (see Sec IV).

We assume a harmonic excitation $p_A(t)=P_A\sin(\omega t)$, where $\omega=2\pi f$ with f being the driving frequency, and P_A the acoustic pressure amplitude. For small oscillation $R=R_0+X$, one can linearize Eq. (13) or (14) in X to obtain a damped simple harmonic oscillator:

$$\ddot{X}+\frac{\dot{X}}{\rho R_0^2}\left(4\mu+\frac{4\kappa^s}{R_0}\right)+\frac{X}{\rho R_0^2}\left(3kP_0-\frac{4\gamma_0}{R_0}+\frac{4E^s}{R_0}\right)=\frac{P_A}{\rho R_0}\sin\omega t, \tag{17}$$

or

$$\ddot{X}+\frac{\dot{X}}{\rho R_0^2}\left(4\mu+\frac{4\kappa^s}{R_0}\right)+\frac{X}{\rho R_0^2}\left[3kP_0+\frac{2\gamma}{R_0}(3k-1)\right]=\frac{P_A}{\rho R_0}\sin\omega t, \tag{18}$$

respectively, for viscoelastic and Newtonian models. The corresponding resonance frequencies are

$$\omega_0^2=\frac{1}{\rho R_0^2}\left(3kP_0-\frac{4\gamma_0}{R_0}+\frac{4E^s}{R_0}\right),$$
$$\omega_0^2=\frac{1}{\rho R_0^2}\left[3kP_0+\frac{2\gamma}{R_0}(3k-1)\right]. \tag{19}$$

Note that the expression for resonance frequency in case of Newtonian rheology is the same as that of a free bubble (see Leighton, 1994, p. 183). The damping term is the same for both models and has an additional interface term compared to the free bubble case (Hoff *et al.*, 2000; Medwin, 1977):

$$\delta_{\text{total}}=\delta_{\text{liquid}}+\delta_{\text{interface}}+\delta_{\text{radiation}},\quad \delta_{\text{liquid}}=\frac{4\mu}{\rho\omega_0R_0^2},$$
$$\delta_{\text{interface}}=\frac{4\kappa^s}{\rho\omega_0R_0^3},\quad \delta_{\text{radiation}}=\frac{\omega^2R_0}{\omega_0c}. \tag{20}$$

Note that we have assumed the surrounding liquid to be incompressible, and thereby do not obtain the radiation damping terms in Eq. (17) or (18). However, including it by the standard prescription (20) does not change the parameter values significantly. The extinction cross section $\sigma_e^{(l)}$ for the linearized dynamics is

$$\sigma_e^{(l)}=4\pi R_0^2\frac{c\,\delta_{\text{total}}}{\omega_0R_0}\frac{\Omega^2}{[(1-\Omega^2)^2+\Omega^2\delta_{\text{total}}^2]}, \tag{21}$$

where $\Omega=\omega/\omega_0$ and c is the sound speed in surrounding liquid [see, e.g., Sarkar and Prosperetti (1994)].

The power absorbed and scattered by microbubbles in frequency domain leads to attenuation $\alpha(\omega)$ in dB/distance

$$\alpha(\omega)=10\log_{10}e\int_{a_{\min}}^{a_{\max}}\sigma_e(a;\omega)n(a)da, \tag{22}$$

where e is the base of natural logarithm, $n(a)da$ is the number of bubbles per unit volume with radius in $(a,a+da)$, and $a_{\max(\min)}$ is the maximum (minimum) value of the range of bubble radii. For the case of N bubbles per unit volume of a uniform size the integral simplifies to $N\sigma_e$. Sonazoid has a relatively narrow size distribution with an average diameter of 3.2 μm and number concentration of 0.78×10^9/ml [Sontum et al. (1999), see also Hoff (2000)]. Notice that $\alpha(\omega)$ is a function of the unknown bubble parameters (γ,κ^s) or (γ_0,E^s,κ^s). The experimental measurement of attenuation over a range of frequencies $\alpha^{\text{meas}}(\omega)$ is used to define an error $\text{Er}(\gamma,\kappa^s)$ or $\text{Er}(\gamma_0,E^s,\kappa^s)$:

$$\mathrm{Er}(\gamma, \kappa^s, \ldots) = \sum_i [\alpha(\omega_i) - \alpha^{\mathrm{meas}}(\omega_i)]^2. \quad (23)$$

The error is minimized to obtain the bubble parameters. MATLAB was used to execute the error minimization. The uncertainty in the estimated parameters is determined by finding the range for which the error residual reaches its minimum value. Similar method is used by previous authors for obtaining model parameters (e.g., Chatterjee and Sarkar, 2003; Hoff *et al.*, 2000).

C. Liquid compressibility and bubble breakup

We have neglected liquid compressibility in our model as did several other research groups (Church, 1995; de Jong *et al.*, 1992; de Jong and Hoff, 1993). To investigate the compressibility effect, we implemented a Keller–Herring type model to find that the model parameters do not vary substantially (see Sec. IV). For brevity, we omitted here a detailed description of the compressible model. Khismatullin and Nadim (2002) have also found that the compressibility and viscoelasticity of the surrounding liquid do not play significant role in the bubble dynamics. Prosperetti (1984) has discussed the suitability of different models of bubble dynamics in case of free bubbles. He has shown that for low Mach Numbers (based on bubble wall velocity) all models with and without compressibility work equally well. Contrast microbubbles are much stiffer compared to a free bubble of the same size, thereby significantly restricting bubble wall motion except at violent collapse. Sboros *et al.* (2002) have observed that at higher amplitudes of excitation incompressible Rayleigh–Plesset model does not perform well (see Sec IV). After determining the properties of Sonazoid, our numerical computation shows that the highest Mach number attained is less than 0.3, except for rare extreme cases, further justifying the assumption of incompressibility. The encapsulation of a contrast microbubble may rupture at high acoustic pressure amplitude, an effect not accounted for in our model.

IV. RESULTS AND DISCUSSION

A. Attenuation measurement and characterization

As was mentioned before, we take Sonazoid as a test case of available ultrasound contrast agent. Attenuation measurement for varying concentration of Sonazoid is shown in Fig. 3(a). The peak attenuation plotted against concentration in Fig. 3(b) displays a linear increase indicating that individual contributions of bubbles are additive, and interactions between them negligible [the void fraction of microbubbles is $\sim 10^{-6}$, which is too small for interaction, Commander and Prosperetti (1989)]. The method outlined in Sec. III B was used to determine interfacial properties for Sonazoid based on the experimental data (for the highest attenuation) of Fig. 3.

Figure 4 shows the Newtonian and viscoelastic models fitted to the experimentally measured attenuation. In the same figure, we also present the curve fit for the Church–Hoff model [Hoff *et al.* (2000); Eq. (6) in their paper] that assumes a 4-nm-thick layer of rubbery incompressible material. The encapsulation material in this model is characterized by a bulk shear modulus G_s, and a shear viscosity μ_s. The parameters determined for each model are presented in Table I. For the viscoelastic model, uncertainty range in γ_0 is not provided, because its variation leads to little change in the residual. Introducing compressibility in the Newtonian

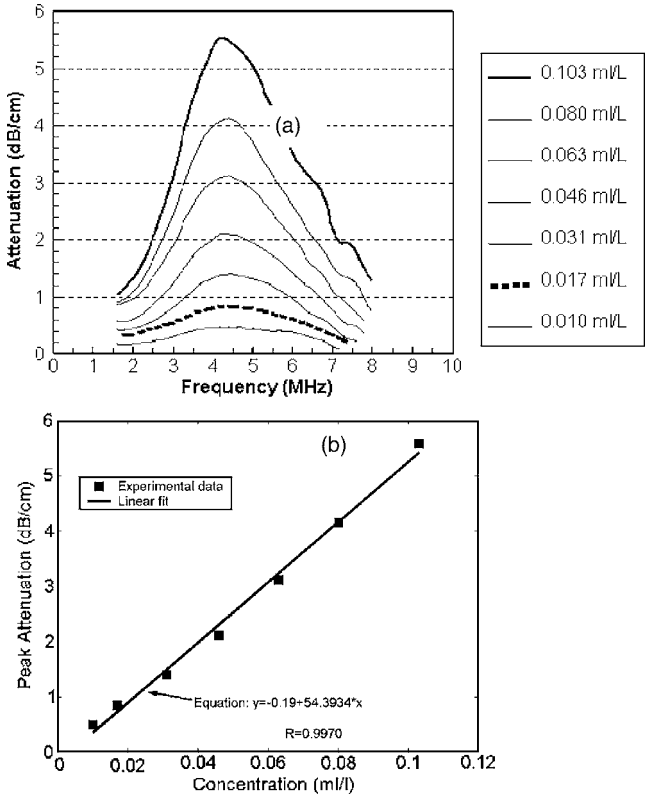

FIG. 3. (a) Attenuation at different concentrations of Sonazoid with one-cycle 5 MHz insonation. The experiments were conducted around 2 min after injections of 0.103, 0.080, 0.063, 0.046, 0.031, 0.017, 0.010 ml/l of Sonazoid in Isoton II (from top to bottom). (b) Variation of peak attenuation with concentration showing the linearity of attenuation with concentration.

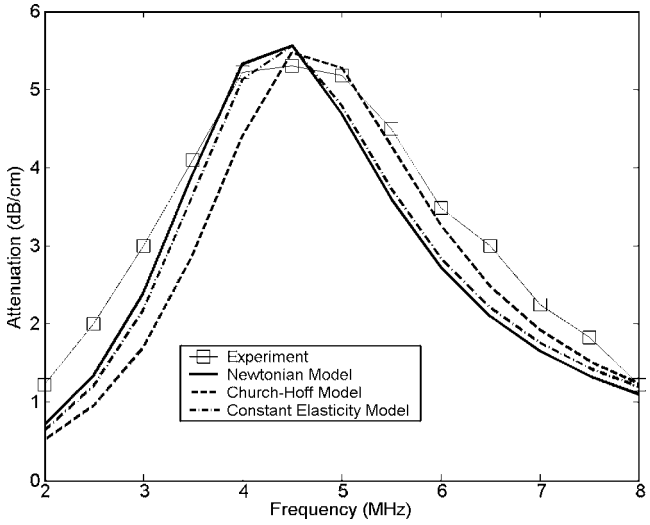

FIG. 4. Determination of the interface (Newtonian and viscoelastic models) and shell (in case of Church–Hoff's model) parameters corresponding to Sonazoid bubbles. Data correspond to a concentration of 0.103 ml/l of Sonazoid in Isoton-II.

TABLE I. Values of parameters estimated for Sonazoid using three different models.

	Newtonian model		Church–Hoff model		Constant elasticity model		
	$\kappa^s(msP=10^{-6}$ Ns/m)	γ(N/m)	G_s(MPa)	μ_s(Pa s)	$\kappa^s(msP=10^{-6}$ Ns/m)	γ_0(N/m)	E^s(N/m)
Mean	0.01	0.6	52	0.99	0.01	0.019	0.51
Range (about mean)	±0.0038	±0.14	±10	±0.3	±0.0038	…	±0.11

model resulted in $\kappa^s=0.012$ msP and $\gamma=0.54$ N/m, not substantially different from their incompressible counterparts. It may be noted that the values obtained for Church–Hoff model are close to those obtained by Hoff (2000).

The values of κ^s are similar to those obtained for other surfactant-laden interfaces [see e.g., Edwards *et al.* (1991), p. 241]. However, γ for the Newtonian model is an order of magnitude higher than that at the gas–water interface (at an air–water interface $\gamma=0.072$ N/m), a result very similar to what we obtained for contrast agent Optison (Chatterjee and Sarkar, 2003). As explained in Sec. III, the high value is a result of the Newtonian model with no explicit elastic term. The elastic contributions are all lumped into the surface tension. The interfacial parameters obtained with the viscoelastic interfacial rheology (containing an explicit dilatational elasticity term) substantiates this explanation. With this model we get $\gamma_0=0.019$ N/m, a value lower than that at the air–water interface. Note that the surface dilatational viscosity κ^s remains the same in these two interface models, as it should if the property represents a physical nature of the encapsulation and not just a mathematical fitting constant. Also surface tension γ in the Newtonian model is indeed a combination of surface tension and dilatational elasticity of the viscoelastic model—$\gamma_{\text{viscous}} \simeq (\gamma_0+E^s)_{\text{viscoelastic}}$. Parameters for three different models are obtained by fitting their linearized versions with the experimentally observed attenuation. In the following, we provide a detailed comparative study of these model behaviors and their ability to predict measurements from a different experiment, viz. scattering.

B. Experimental measurements of scattered fundamental and subharmonic emissions

We measure scattering of ultrasound through solution of Sonazoid at different driving frequencies and pressure amplitudes, and investigate fundamental [Fig. 5(a)] and subharmonic [Fig. 5(b)] scattered responses. The fundamental response increases linearly with exciting acoustic pressure for lower pressures, but saturates at higher pressures (e.g., above 0.6 MPa for 2 MHz insonation). Furthermore, it decreases with increasing excitation frequency. The saturation in fundamental response is due to the nonlinear energy transfer into other frequencies at higher excitations, as well as possible breakup.

Figure 5(b) shows that a subharmonic response roughly has three different regimes with increasing pressure amplitudes—initial slow increase, rapid growth, and saturation. It may be pointed out that similar trends were also observed in the case of Optison (Shi *et al.*, 1999). During initiation, the subharmonic component is insignificant (near the noise level, e.g., for pressures less than 0.3 MPa at 6 MHz insonation). During growth, the subharmonic response increases rapidly with the acoustic pressure, and usually has amplitudes much above the background noise. As the acoustic pressure increases further (e.g., 0.8 MPa for 6 MHz insonation), the growth of the subharmonic component saturates. At this stage, the variation in the data is substantially high possibly indicating chaotic response due to inertial cavitation (Shi *et al.*, 1999; also see Prosperetti, 1975; Apfel and Holland, 1991) Note that the first two regimes roughly coincide with the linear growth of the fundamental response in Fig. 5(a). For higher frequencies, the initiation of growth is

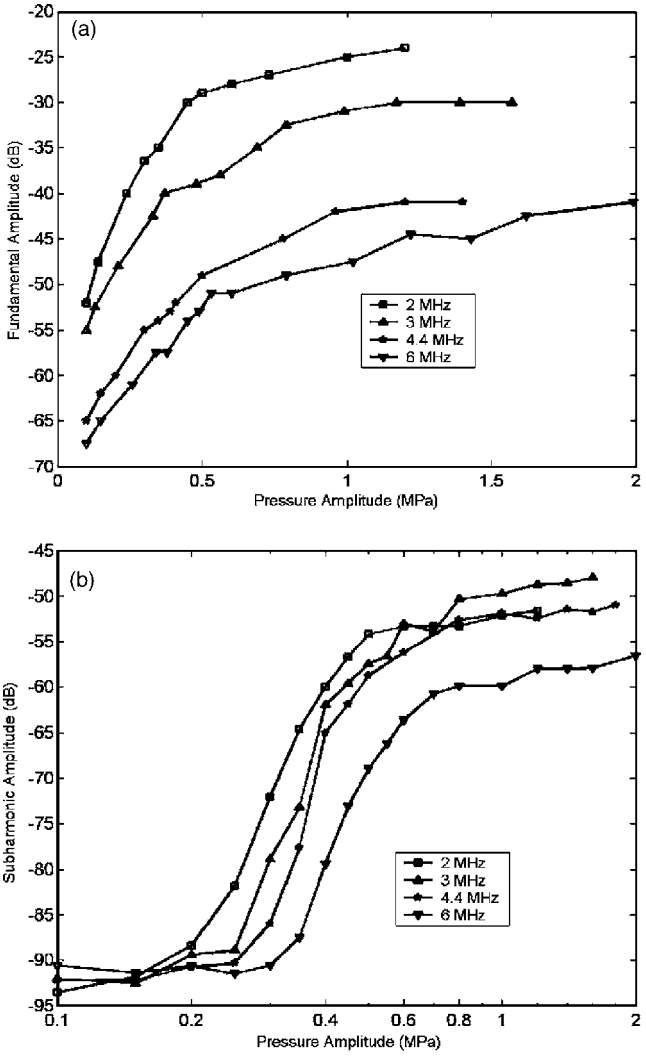

FIG. 5. Scattered fundamental (a) and subharmonic (b) response of Sonazoid vs transmitted acoustic pressure amplitudes at different insonication frequencies. Averaged values of four data sets were used for 2.0 MHz insonication and averaged values of eight data sets were used for 3.0, 4.4, and 6.0 MHz insonication.

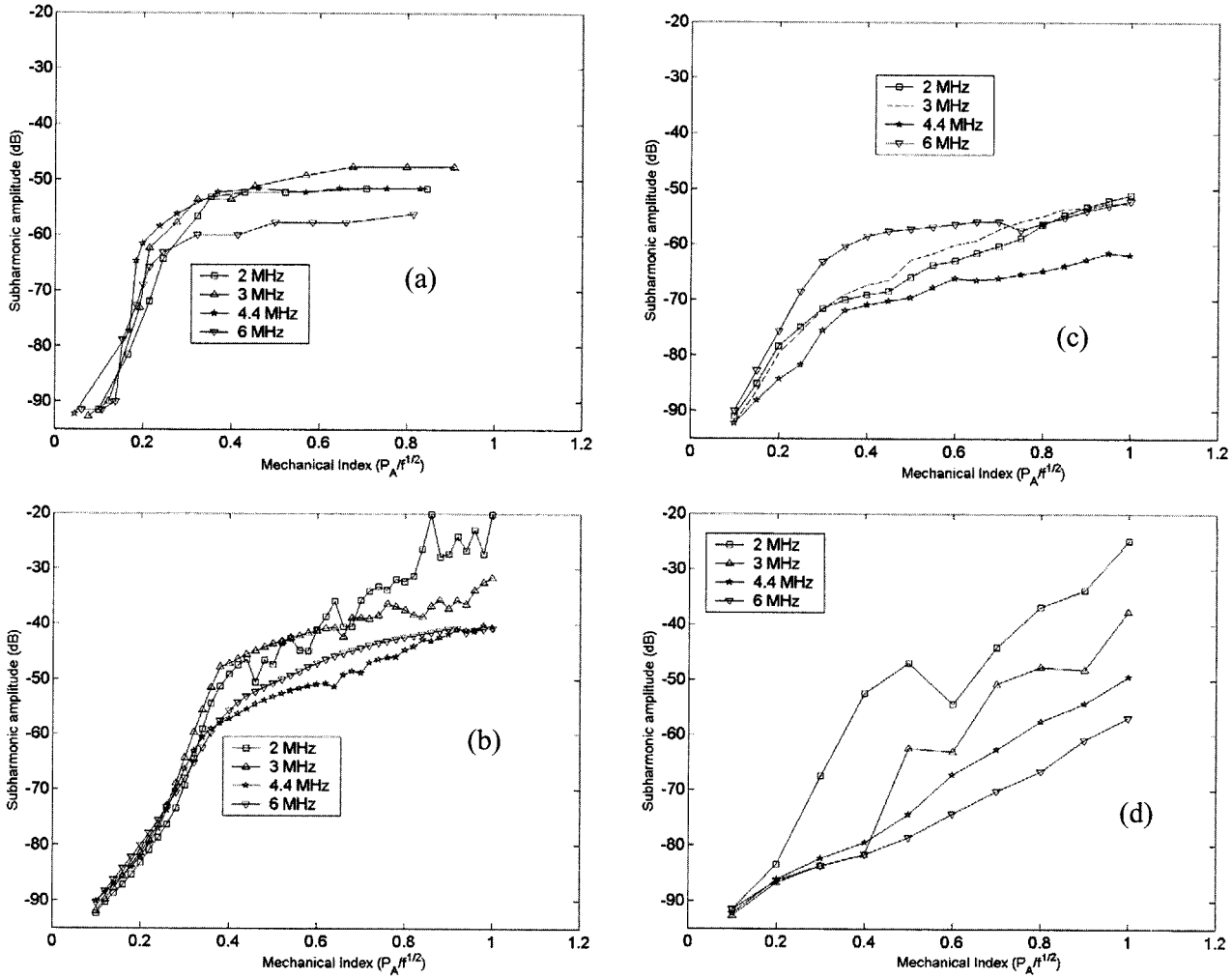

FIG. 6. (a) Subharmonic response against MI. (a) Experimental data [as presented in Fig. 5(b)], (b) simulation with Newtonian viscous model, (c) with Church–Hoff model, and (d) with viscoelastic model.

progressively delayed, and the subharmonic response is decreased. In case of a free bubble, a similar sharp initiation is observed for subharmonic response in contrast to superharmonic responses, which show continuous and gradual increase with pressure amplitudes (Eller and Flynn, 1969). Mechanical index MI=$P_A/f^{1/2}$ [P_A, the pressure amplitude measured in MPa and frequency (f) in MHz] is often used as a criterion for cavitation (Apfel and Holland, 1991). On the other hand detectable subharmonic response has been suggested as an experimental signature of cavitation (Prosperetti, 1975). Note that MI is a rough estimate of the energy of the excitation as well. One would therefore expect the subharmonic response to correlate with MI. In Fig. 6(a), we plot the subharmonic response for different frequencies as a function of MI. Such a rescaling of pressure with $f^{1/2}$ shows a collapse of the data for different frequencies at least in the rapid growth region [Fig. 6(a)]. However, the scaling is poor in the saturation region.

C. Model predictions and comparison of fundamental and subharmonic scattering

We use Rayleigh–Plesset equation (13) or (14) with model parameters determined by the procedure described in Sec. III B to simulate microbubble dynamics. The far-field scattering is computed from the time evolution of bubble radius using Eq. (16) followed by extraction of fundamental and subharmonic responses using FFT. They are compared to experimental observations. The simulation is scaled to match the experimental data for the lowest pressure level. Note that the model parameters were determined using attenuation with a linearized equation valid only for small oscillations. The underlying assumption is that the determined material properties retain their validity for different types of experiments (scattering or attenuation), and also remain constant in a range of magnitude of oscillation (they may change for large oscillation leading to, e.g., shear rate dependent interface viscosity/elasticity and interfacial tension).

In Figs. 6(b), 6(c), and 6(d) we plot the scattered subharmonic response with MI predicted by the Newtonian, Church–Hoff, and viscoelastic models. We find that the Newtonian model performs the best among three in capturing the observed collapse in Fig. 6(a) of subharmonic response for different frequencies. Next we perform a detailed comparison between observed scatterings at different frequencies and corresponding predictions of the three models—Fig. 7 for fundamental and Fig. 8 for subharmonic emissions. All mod-

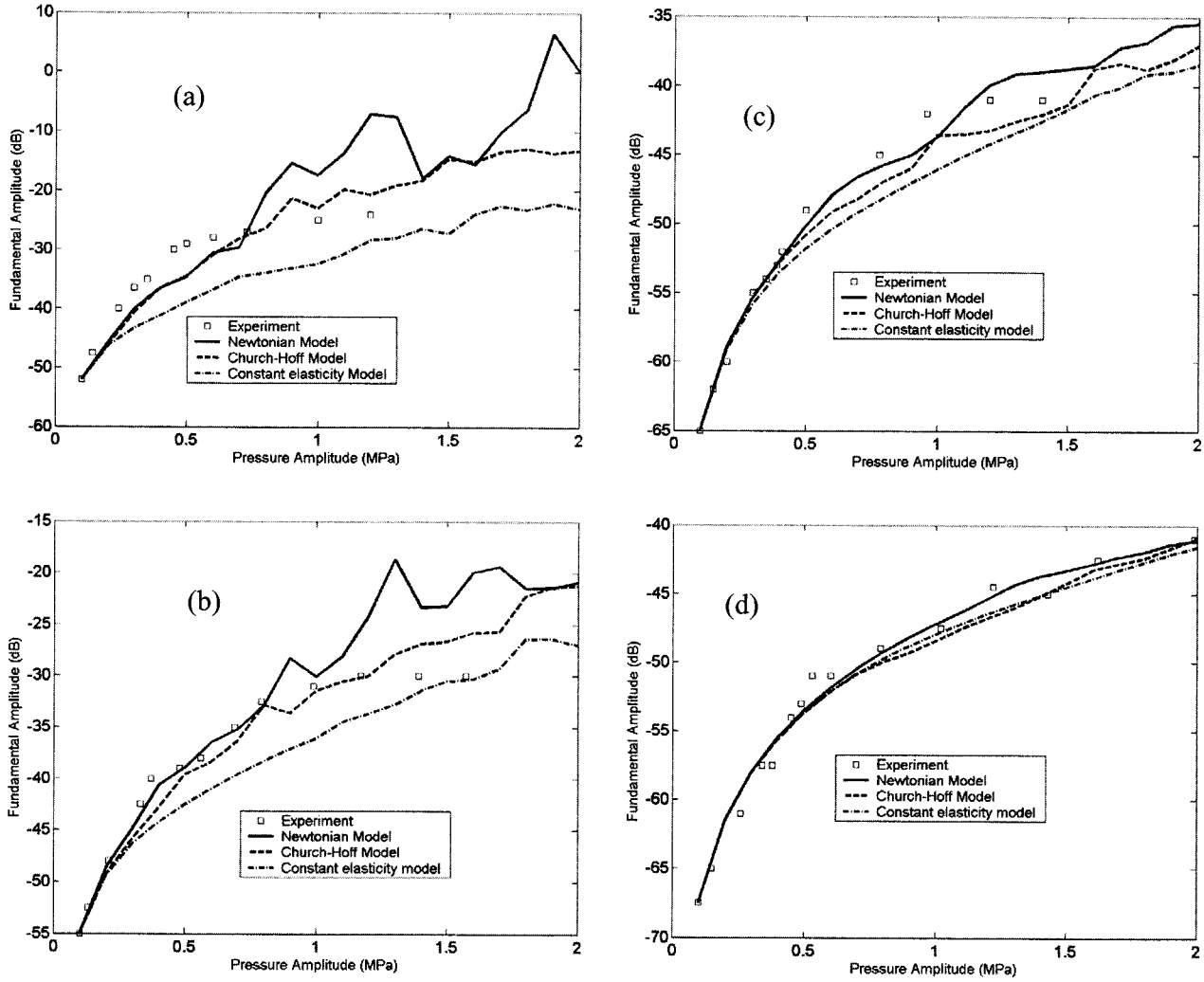

FIG. 7. Predicted and measured first harmonic response for Sonazoid at various insonation frequencies: (a) 2 MHz, (b) 3 MHz, (c) 4.4 MHz, and (d) 6 MHz.

els show fundamental response increasing with the acoustic pressure in keeping with the experiment. The Newtonian and the Church–Hoff models perform marginally better than the viscoelastic one. For the subharmonic data (Fig. 8), the Newtonian model provides the best match with experiment except at the highest frequency, 6 MHz, where Church–Hoff model predicts better than the other two. For all frequencies, the viscoelastic model predicts much less scattering than has been observed. Note that all models are fitted with a linear analysis and with a low amplitude attenuation data. The relative failure of the viscoelastic model at higher excitation might result from a very stiff encapsulation with a large surface dilatational elasticity. However, at higher excitations when bubble experiences larger excursion of the bubble surface, the encapsulation might "soften" with a far lower value of surface dilatational elasticity, not included in the model. One could incorporate a softening in the elasticity (by assuming, e.g., a nonlinear dilatational elasticity) to account for that. Note that the Newtonian model even with a high surface tension term (dilatational elasticity and interfacial tension lumped into one) predicts subharmonic response very well. The bubble dynamics with Newtonian (14) and viscoelastic (13) rheologies are remarkably similar, except for the elastic terms (surface tension and surface dilatational elasticity); they are matched and thereby produce the same results at small excitations. However, at higher excitations the Newtonian model (14) is far less stiff than the other one. Figures 6–8 show that all models display fine structures for some frequency values in their predictions especially for stronger excitations absent in their experimental counterparts. The structures are signatures of "near-chaotic" response in the bubble dynamics equations. Note that for strong excitations, the bubbles experience nonspherical oscillations, inertial cavitation, and possible breakup not included in any of the models considered here.

V. SUMMARY

We have presented a procedure to characterize encapsulated microbubble based ultrasound contrast agent through controlled *in vitro* attenuation and scattering experiments and analytical models. We applied it to contrast agent Sonazoid (GE Healthcare; Oslo, Norway) using three models for the bubble encapsulation. We have developed zero-thickness interface models with their intrinsic interfacial rheology. Here we presented two different rheological models-(1) *Newton-*

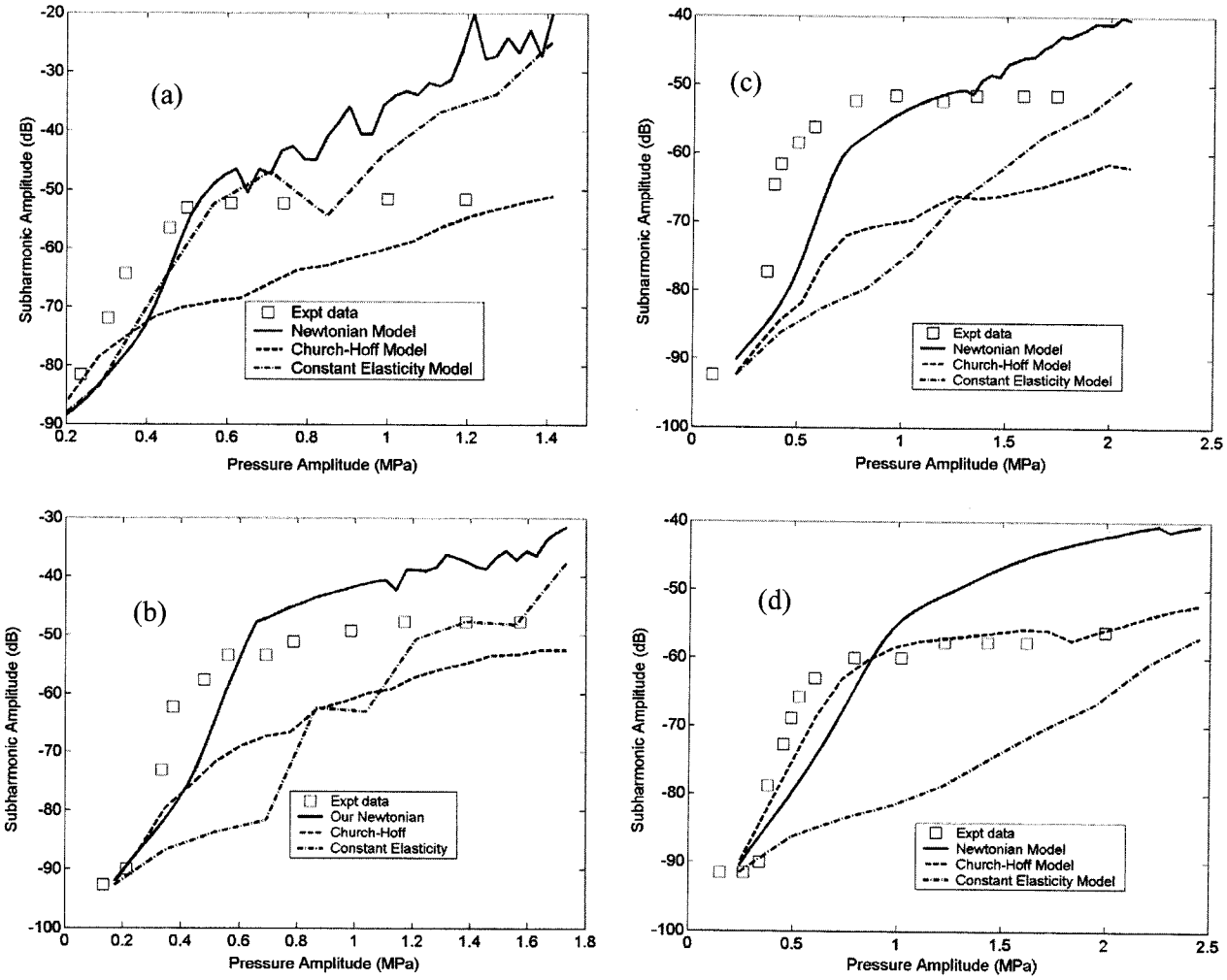

FIG. 8. Predicted and measured subharmonic response for Sonazoid at various insonation frequencies: (a) 2 MHz, (b) 3 MHz, (c) 4.4 MHz, and (d) 6 MHz.

ian (surface tension γ, dilatational surface viscosity κ^s) and (2) *viscoelastic* (surface tension γ_0, surface dilatational viscosity κ^s, and surface dilatational elasticity E^s). The rheological properties for the models were determined by comparing predictions of a linearized dynamics with attenuation measured at small excitations. The characteristic rheological properties for Sonazoid were $\gamma=0.6$ N/m, $\kappa^s=0.01$ msP($=10^{-6}$ Ns/m) for the Newtonian model. The abnormally high value of the interfacial tension motivated our viscoelastic model. The viscoelastic model results in $\kappa^s=0.01$ msP, $\gamma_0=0.0190$ N/m, a value indeed much lower than that (~ 0.07 N/m) at the air–water interface, and $E^s=0.51$ N/m. The value of dilatational viscosity remains the same for both models. For comparison, we also implemented a model due to Church (Church, 1995; Hoff *et al.*, 2000) that assumes a layer of finite thickness (4 nm) containing rubbery incompressible material for the encapsulation. It is characterized by bulk material properties (shear modulus G_s, and shear viscosity μ_s). For Sonazoid properties are $G_s=52$ MPa and $\mu_s=0.99$ Pa s.

We measured scattered fundamental and subharmonic responses from a Sonazoid solution at different frequencies and amplitudes of excitation, and compared them with predictions of the three models considered. For all frequencies, the fundamental response grows linearly for small values of excitations before slowing down at higher values, a feature matched well by all three models. The measured subharmonic emission displayed rapid growth beyond a critical pressure amplitude. The growth region of subharmonic emission scales with $P_A/f^{1/2}$, i.e., the mechanical index (MI). The resulting collapse of subharmonic response with MI for various frequencies is captured well only by the Newtonian model. The performance of the Newtonian model is better than the other two in matching the subharmonic response for most frequencies. The viscoelastic model consistently underpredicted the subharmonic response at all frequencies. We surmise that the high value of surface dilatational elasticity determined using the linear analysis of the low amplitude attenuation data has made a stiff encapsulation resulting in a lower response at higher excitation. A "softening" of the encapsulation by assuming a surface dilatational elasticity constant that decreases with fractional area increase can be a possible remedy. The comparative investigation delineates predictive capability of the three models for experimental responses that are different from those used to obtain the parameters. Further model development and their applications to other contrast agents will be the subject of future work.

ACKNOWLEDGMENTS

The authors acknowledge support from DOD Contract No. DAMD17-03-1-0119. K.S. acknowledges University of Delaware Research Foundation and NSF Contract No. CTS-0352829. K.S. also acknowledges editorial help from Pankaj Jain.

Apfel, R. E. and Holland, C. K. (**1991**). "Gauging the likelihood of cavitation from short-pulse low-duty cycle of diagnostic ultrasound," Ultrasound Med. Biol. **17**, 179–185.

Brennen, C. E. (**1995**). *Cavitation and Bubble Dynamics* (Oxford University Press, New York).

Chang, P. H., Shung, K. K., and Levene, H. B. (**1996**). "Quantitative measurements of second harmonic Doppler using ultrasound contrast agents," Ultrasound Med. Biol. **22**, 1205–1214.

Chatterjee, D. and Sarkar, K. (**2003**). "A Newtoninan rheological model for the interface of microbubble contrast agents," Ultrasound Med. Biol. **29**, 1749–1757.

Chen, W. S., Matula, T. J., Brayman, A. A., and Crum, L. A. (**2003**). "A comparison of the fragmentation thresholds and inertial cavitation doses of different ultrasound contrast agents," J. Acoust. Soc. Am. **113**, 643–651.

Christiansen, C., Kryvi, H., Sontum, P. C., and Skotland, T. (**1994**). "Physical and biochemical characterization of Albunex™, a new ultrasound contrast agent consisting of air-filled albumin microspheres suspended in a solution of human albumin," Biotechnol. Appl. Biochem. **19**, 307–320.

Church, C. C. (**1995**). "The effects of an elastic solid surface layer on the radial pulsations of gas bubbles," J. Acoust. Soc. Am. **97**, 1510–1521.

Commander, K. W. and Prosperetti, A. (**1989**). "Linear pressure waves in bubbly liquids-comparison between theory and experiments," J. Acoust. Soc. Am. **85**, 732–746.

de Jong, N., Cornet, R., and Lancèe, C. T. (**1994**). "Higher harmonics of vibrating gas-filled microspheres. Part two: Measurements," Ultrasonics **32**, 455–459.

de Jong, N. and Hoff, L. (**1993**). "Ultrasound scattering properties of Albunex microspheres," Ultrasonics **31**, 175–181.

de Jong, N., Hoff, L., Skotland, T., and Bom, N. (**1992**). "Absorption and scatter of encapsulated gas filled microspheres: Theoretical consideration and some measurements," Ultrasonics **30**, 95–103.

Devin, C. (**1959**). "Survey of thermal, radiation and viscous damping of pulsating air bubbles in water," J. Acoust. Soc. Am. **31**, 1654–1667.

Edwards, D. A., Brenner, H., and Wasan, D. T. (**1991**). *Interfacial Transport Processes and Rheology* (Butterworth-Heinemann).

Eller, A. I. (**1970**). "Damping constants of pulsating bubbles," J. Acoust. Soc. Am. **47**, 1469–1470.

Eller, A. and Flynn, H. G. (**1969**). "Generation of subharmonic of order one-half by bubbles in a sound field," J. Acoust. Soc. Am. **46**, 722–727.

El-Sherif, D. M. and Wheatley, M. A. (**2003**), "Development of a novel method for synthesis of a polymeric ultrasound contrast agent,"J. Biomed. Mater. Res. **66A**, 347–355.

Epstein, P. S. and Plesset, M. S. (**1950**). "On the stability of gas bubbles in liquid-gas solutions," J. Chem. Phys. **18**, 1505–1509.

Evans, E. A. and Skalak, R. (**1980**). *Mechanics and Thermodynamics of Biomembranes*(CRC Press, Boca Raton, FL).

Frinking, P. J. A., Boukaz, A., Kirkhorn, J., Ten Cate, F. J., and de Jong, N. (**2000**). "Ultrasound contrast imaging: Current and new potential methods," Ultrasound Med. Biol. **26**, 965–975.

Frinking, P. J. A. and de Jong, N. (**1998**). "Acoustic modeling of shell-encapsulated gas bubbles," Ultrasound Med. Biol. **24**, 523–533.

Goldberg, B. B., Raichlen, J. S., and Forsberg, F. (**2001**). *Ultrasound Contrast Agents: Basic Principles and Clinical Applications*, 2nd ed. (Martin Dunitz, London).

Graham, D. E. and Phillips, M. C. (**1980**). Proteins at liquid interfaces. IV. Dilatational properties," J. Colloid Interface Sci. **70**, 227–239; "Proteins at liquid interfaces. V. Shear properties," J. Colloid Interface Sci. **70**, 239–250.

Hilgenfeldt, S., Lohse, D., and Zomack, M. (**1998**). "Response of bubbles to diagnostic ultrasound: A unifying theoretical approach," Eur. Phys. J. B **4**, 247–255.

Hoff, L. (2000). "Acoustic characterization of contrast agents for medical ultrasound imaging," Ph.D. thesis, Norwegian University of Science and Technology.

Hoff, L., Sontum, P. C., and Hovem, J. M. (**2000**). "Oscillations of polymeric microbubbles: Effect of the encapsulating shell," J. Acoust. Soc. Am. **107**, 2272–2280.

Kabalnov, A., Klein, D., Pelura, T., Schutt, E., and Weers, J. (**1998**). "Dissolution of multicomponent microbubbles in the bloodstream. 1. Theory," Ultrasound Med. Biol. **24**, 739–749.

Khismatullin, D. B. and Nadim, A. (**2002**). "Radial oscillations of encapsulated microbubbles in viscoelastic liquids," Phys. Fluids **14**, 3534–3557.

Kralchevsky, P. A. and Nagayama, K. (**2001**). *Particles at Fluids Interfaces and Membranes*, Studies in Interface Science Vol. **10** (Elsevier, Amsterdam, The Netherlands).

Leighton, T. G. (**1994**). *The Acoustic Bubble* (Academic, San Diego).

May, D. J., Allen, J. S., and Ferrara, K. W. (**2002**). "Dynamics and fragmentation of thick-shelled microbubbles," IEEE Trans. Ultrason. Ferroelectr. Freq. Control **49**, 1400–1410.

Medwin, H. (**1977**). "Counting bubbles acoustically: A review," Ultrasonics **15**, 7–13.

Moran, C. M., Watson, R. J., Fox, K. A. A., and McDicken, W. N. (**2002**). "In vitro acoustic characterization of four intravenous ultrasonic contrast agents at 30 MHz," Ultrasound Med. Biol. **28**, 785–791.

Morgan, K. E., Allen, J. S., Dayton, P. A., Chomas, J. E., Klibanov, A. L. and Ferrara, K. W. (**2000**). "Experimental and theoretical evaluation of microbubble behavior: Effect of transmitted phase and bubble size," IEEE Trans. Ultrason. Ferroelectr. Freq. Control **47**, 1494–1509.

Myrset, A. H., Nicolaysen, H., Toft, K., Christiansen, C., and Skotland, T. (**1996**). "Structure and organization of albumin molecules forming the shell of air-filled microspheres: Evidence for a monolayer of albumin molecules of multiple orientations stabilizing the enclosed air," Biotechnol. Appl. Biochem. **24**, 145–153.

Prosperetti, A. (**1975**). "Nonlinear oscillation of gas bubbles in liquids: Transient solutions and the connection between subharmonic signal and cavitation," J. Acoust. Soc. Am. **57**, 810–821.

Prosperetti, A. (**1984**). "Bubble phenomena in sound fields. Part one," Ultrasonics **22**, 69–78.

Sarkar, K. and Prosperetti, A. (**1994**). "Coherent and incoherent scattering by oceanic bubbles," J. Acoust. Soc. Am. **96**, 332–341.

Sboros, V., MacDonald, C. A., Pye, S. D., Moran, C. M., Gomatam, J., and McDicken, W. N. (**2002**). "The dependence of ultrasound contrast agents backscatter on acoustic pressure: Theory versus experiment," Ultrasonics **40**, 579–583.

Shankar, P. M., Krishna, P. D., and Newhouse, V. L. (**1998**). "Advantages of subharmonic over second harmonic backscatter for contrast-to-tissue echo enhancement," Ultrasound Med. Biol. **24**, 395–399.

Shi, W. T. and Forsberg, F. (**2000**). "Ultrasonic characterization of the nonlinear properties of contrast microbubbles," Ultrasound Med. Biol. **26**, 93–104.

Shi, W. T., Forsberg, F., Hall, A. L., Chiao, R. Y., Liu, J., Miller, S., Thomenius, K. E., Wheatley, M. A., and Goldberg, B. B. (**1999**). "Subharmonic imaging with microbubble contrast agents: Initial results," Ultrason. Imaging **21**, 79–94.

Shi, W. T., Forsberg, F., Tornes, A., Ostensen, J., and Goldberg, B. B. (**2000**). "Destruction of contrast microbubbles and the association with inertial cavitation," Ultrasound Med. Biol. **26**, 1009–1019.

Simpson, D. H., Chin, C. T. and Burns, P. N. (**1999**), "Pulse inversion Doppler: a new method for detecting nonlinear echoes from microbubble contrast agents", IEEE Trans. Ultrason. Ferroelectr. Freq. Control **46**, 372–382.

Sontum, P. C., Østensen, J., Dyrstad, K., and Hoff, L. (**1999**). "Acoustic properties of NC100100 and their relation with the microbubble size distribution," Invest. Radiol. **34**, 268–275.